Electronic Supplementary Material (ESI) for Nanoscale.
This journal is © The Royal Society of Chemistry 2017

Electronic Supporting Information

Polymer sequencing by molecular machines: A framework for predicting the resolving power of a sliding contact force spectroscopy sequencing method.

Alex Dunlop[a], Kate Bowman[b], Olav Aarstad[c], Gudmund Skjåk-Bræk[c], Bjørn T. Stokke[d], Andrew N. Round[b]*

(a) Dr. A. Dunlop
HH Wills Physics Laboratory, University of Bristol, Tyndall Avenue, Bristol BS8 1TL, UK
(b) Dr. K. Bowman, Dr. A. N. Round (*corresponding author; e-mail: a.round@uea.ac.uk)
School of Pharmacy, University of East Anglia, Norwich Research Park, Norwich NR4 7TJ, UK
(c) Dr. O. A. Aarstad, Prof. G. Skjåk-Bræk
Department of Biotechnology, The Norwegian University of Science and Technology, NTNU, NO-7491 Trondheim, Norway
(d) Prof. B. T. Stokke
Department of Physics, The Norwegian University of Science and Technology, NTNU, NO-7491 Trondheim, Norway

1. Single Molecule Force Spectroscopy Analysis

1.1 Data Selection

Force spectroscopy data was first assessed within the JPK processing software. **Figure S1** presents typical force-distance profiles for the systems discussed here and for control experiments. In some cases a sinusoidal pattern was apparent in the baseline of the force curves, reflecting a degree of optical interference arising from scattering of the laser spot on the back of the cantilever. This was corrected for prior to analysis by subtraction. The raw data, before subtraction, is displayed in Figure S1. All force-distance profiles to which the extended freely jointed chain model (eFJC) [S1] could be fit were selected for further analysis. Fits to the eFJC model were performed within the JPK processing software, and values for the free parameters fitted to the model (contour length, breaking force and Kuhn length) were extracted.

Within the data collected, three types of force-distance profiles could be discerned (**Figure 3a**, main text). In the first, found when the CD is pulled along the rotaxane containing stations 1 and 2, there are two stretches with rupture forces of around 50-250 pN separated by a distance of approximately 100nm, between which the force reaches a plateau value approximately 40 pN above the baseline. In the second, found when the CD is pulled along rotaxanes containing stations 4 or 5, there is a single stretching event terminating at a force of approximately 50-

150 pN which may sometimes be preceded by a discernible plateau at around 30-40 pN. The third type of event is found in all experiments and consists of a single stretching event, terminating at a high rupture force (these are the only events to exceed 300 pN). When polymers lacking threaded CDs are used instead of the corresponding rotaxane, and when an AFM probe with no tether is used instead of the NHS-terminated tether, then few events occur and when they do, force-distance profiles of the third type are exclusively observed. In all these experiments, we observed very few short-range non-specific adhesion events. **Figure 3(a)** in the main text shows a selection of force-distance profiles from the systems explored here, with examples of each of first two types of force-distance profiles discussed above.

Plots of breaking force *f* vs. contour length L (**Figure S2**) were inspected in order to identify the force-distance profiles corresponding to sliding over the incorporated stations. In the rotaxane containing stations 1 and 2, a high density of breaking events occur around lengths of 90 ± 20 nm and 200 ± 20 nm, in agreement with the expected positions of stations 2 and 1 respectively as previously shown [S2]. Breaking events that fell within these two length ranges, and which possess a plateau in force preceding the stretching event, were identified as station sliding events and were selected for further analysis. A similar procedure was conducted for the rotaxanes containing stations 4 and 5. Here the oligouronates are attached to shorter PEGs with contour lengths of about 20 nm and a high density of rupture events occurs at the corresponding distance from the surface.

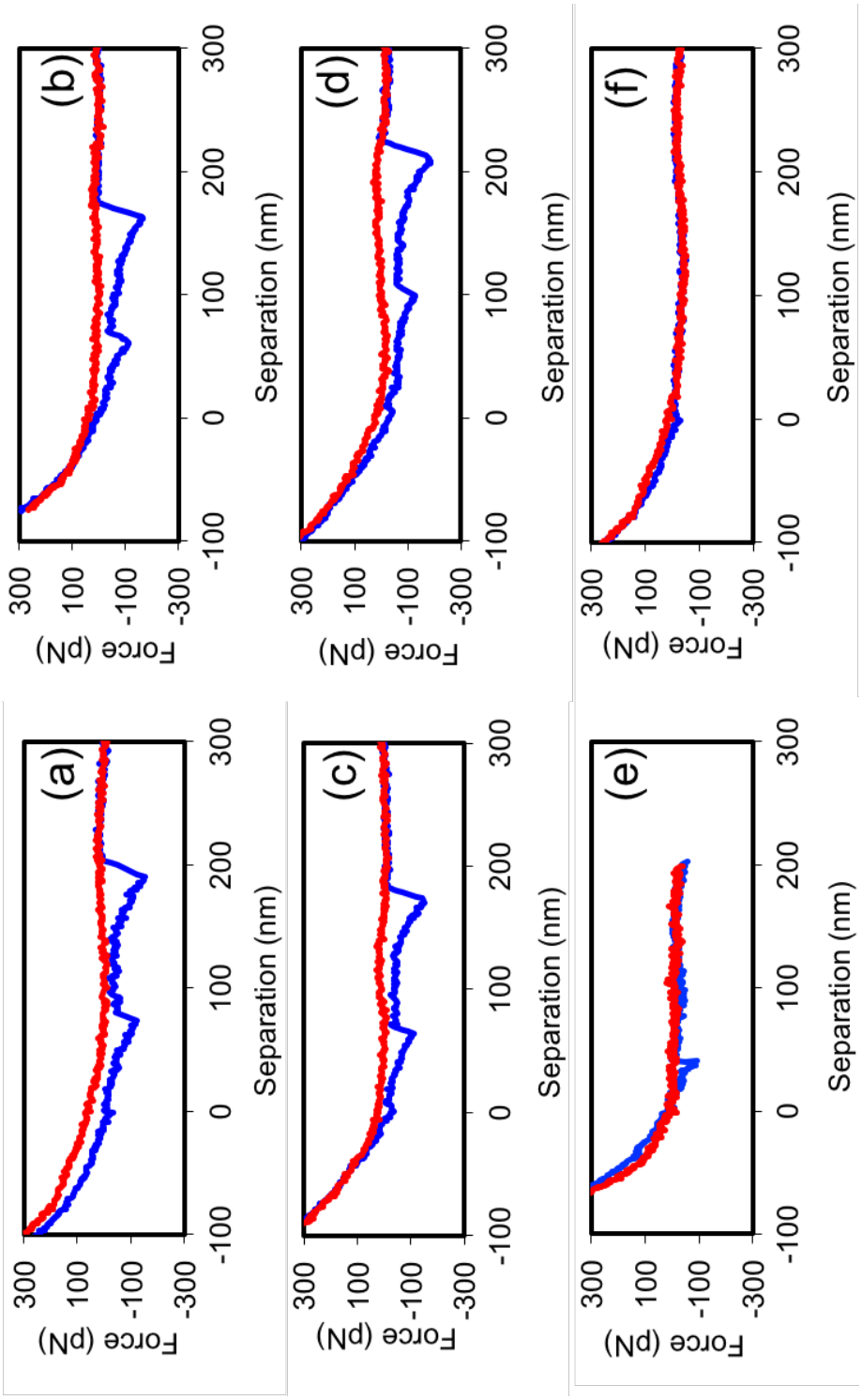

Figure S1. SCFS Force-distance profiles obtained during experiments using AFM probes functionalised with succinimidyl groups and amine-terminated α-CD threaded on to (a-d) polymer conjugates containing stations 1, 2 and 3, and (e) a polymer conjugate consisting of stations 3 and 4. In (f) a control experiment with an unfunctionalised probe and the polymer conjugate containing stations 1,2 and 3 is shown.

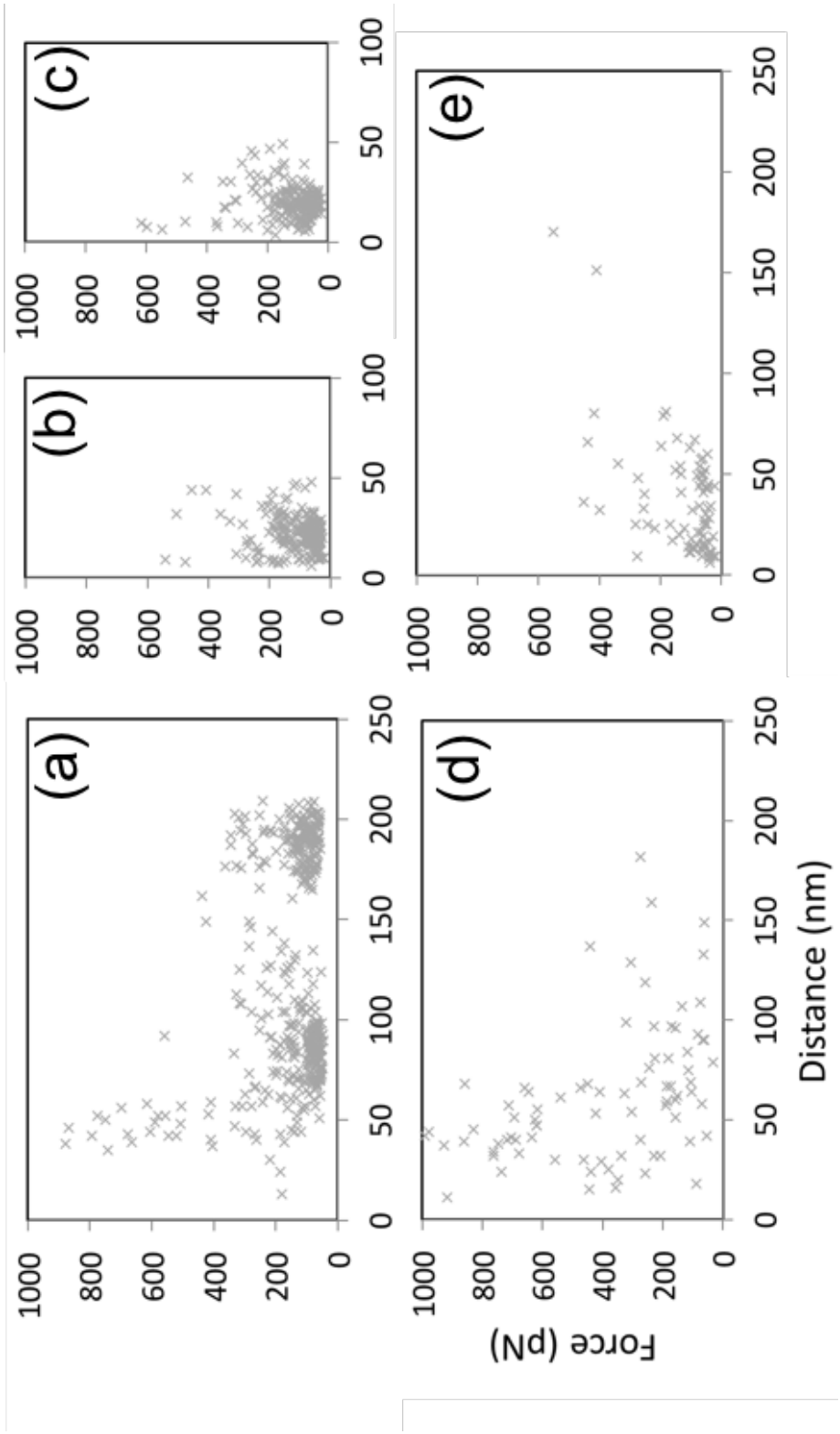

Figure S2. Plots of breaking force (pN) vs distance (nm) for rupture events in the following systems: (a,e) rotaxanes containing α-CD and stations 1, 2 and 3; (b) rotaxanes containing α-CD and stations 3 and 4; (c) rotaxanes containing α-CD and stations 3 and 5; (d) polymers containing stations 1, 2 and 3 but no CD; (e) same as (a) but with a bare tip.

The Kuhn length for a single polyethylene glycol (PEG) polymer (as we use here as a flexible spacer) has been estimated to be 0.7 nm [S3]. Akhremitchev has shown [S4] that the Kuhn length is diagnostic for the presence of a single polymer stretch, since the value of the apparent Kuhn length varies as 1/n, where n = number of simultaneous parallel polymer stretches. **Figure S3** shows plots of rupture force vs. Kuhn length for the rupture events in the rotaxane systems described in this work. In the case of stations 1, 2, 4 and 5, it can be seen that below a Kuhn length value of 0.6 nm there is an increase in the number of high force events, while there are also substantial populations of events with similar forces to the events where the Kuhn length exceeds 0.6 nm. For sliding events involving station 3 the Kuhn length cannot be determined directly so the designated Kuhn length is that found for the sliding event involving one of the other stations that immediately follows the sliding plateau over station 3. **Figure S4** shows that, at comparable loading rates, the stretches fit by Kuhn lengths of 0.6 nm or greater ruptured at lower forces than the stretches fit by Kuhn lengths lower than 0.6 nm. This result is in accordance with the predictions of Akhremitchev and suggests that events with lower Kuhn lengths represent multiple simultaneous (or nearly so) bond ruptures. We therefore selected for further analysis only those events with a Kuhn length of 0.6 nm or greater.

Figure S3 (following page). Plots of Force (pN) vs. Kuhn length (nm) for sliding events for (a) α-CD and (b) β-CD over station 1; (c) α-CD and (d) β-CD over station 2; (e) α-CD and (f) β-CD over station 3; (g) α-CD over station 4 and (h) α-CD over station 5. Crosses represent events fit by a Kuhn length less than 0.6 nm (representing multiple interactions), open circles represent events fit by Kuhn lengths of 0.6 nm or greater (representing single interactions).

Figure S4 (following page)**.** Plots of Force (pN) vs. Loading rate (pN/s) for sliding events for (a) α-CD and (b) β-CD over station 1; (c) α-CD and (d) β-CD over station 2; (e) α-CD and (f) β-CD over station 3; (g) α-CD over station 4 and (h) α-CD over station 5. Note the logarithmic scale of the *x*-axis. Crosses represent events fit by a Kuhn length less than 0.6 nm (representing multiple interactions), open circles represent events fit by Kuhn lengths of 0.6 nm or greater (representing single interactions).

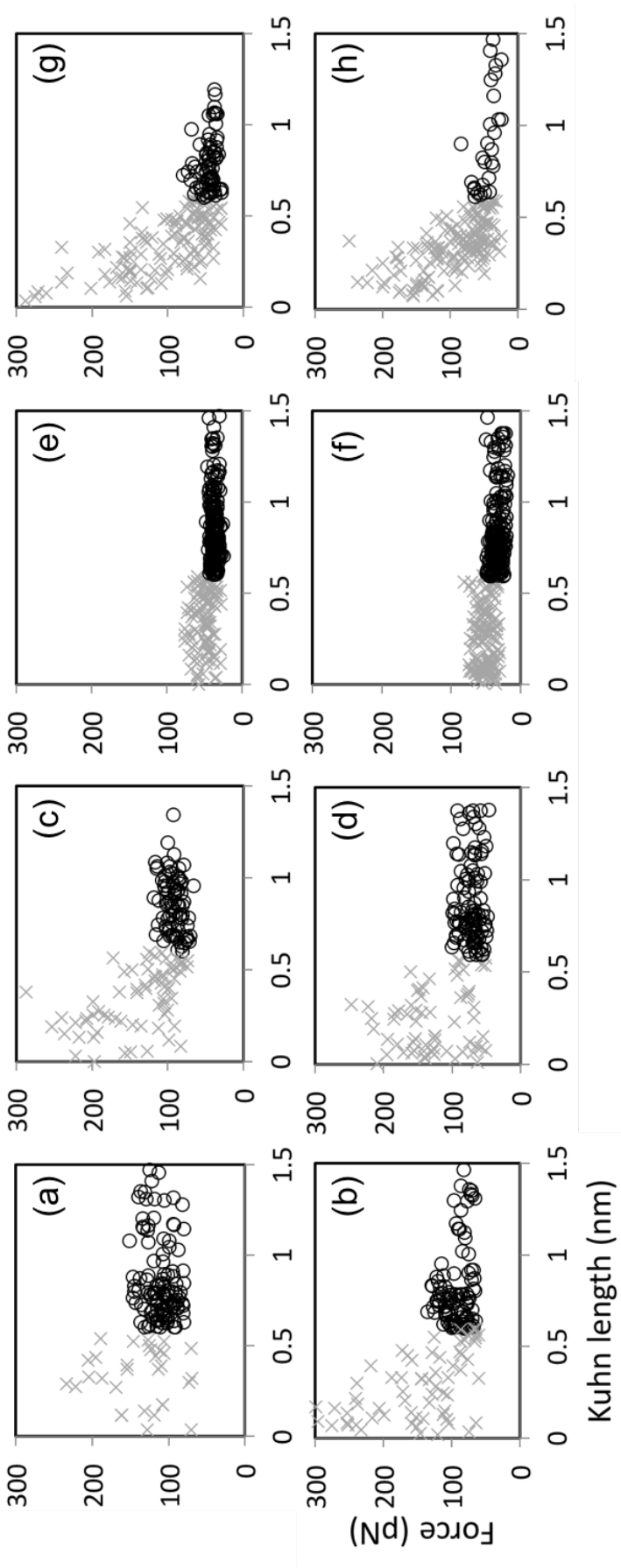

Figure S3.

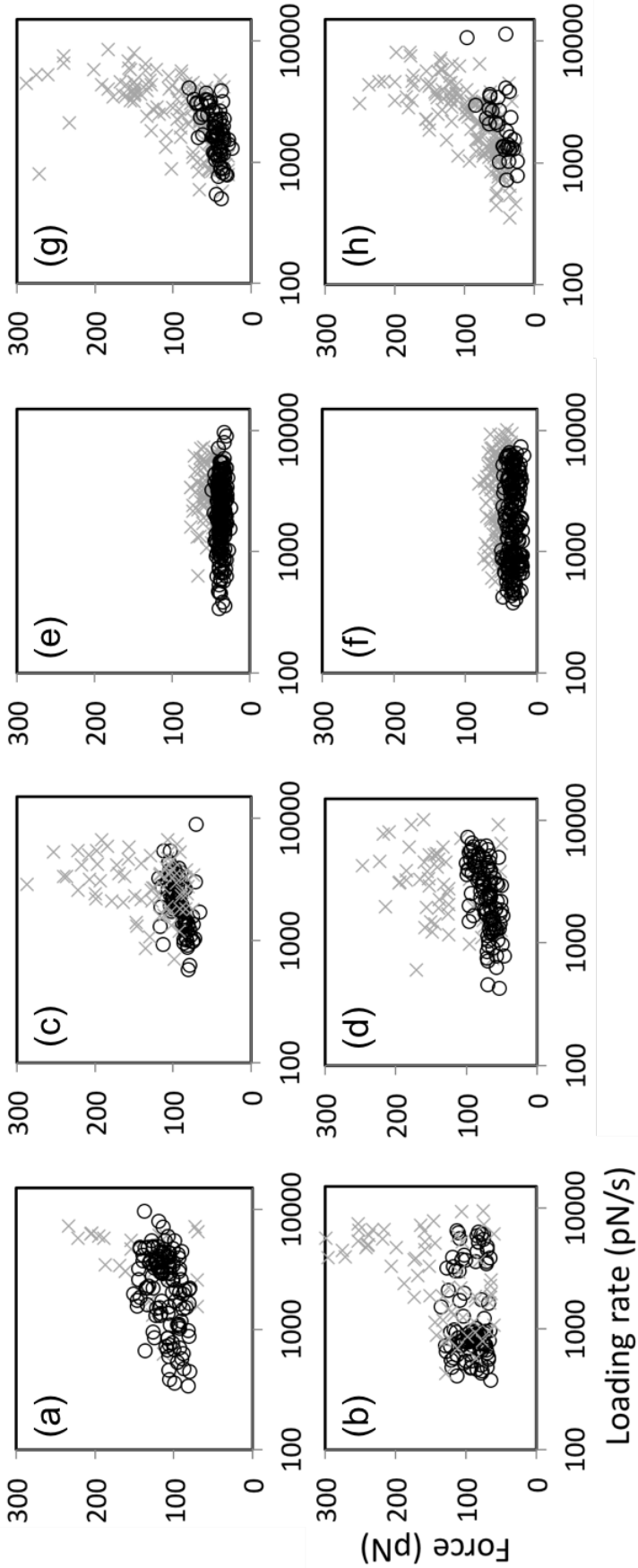
(a)
(b)
(c)
(d)
(e)
(f)
(g)
(h)
Force (pN)
Loading rate (pN/s)
300
200
100
0
100
1000
10000

Figure S4.

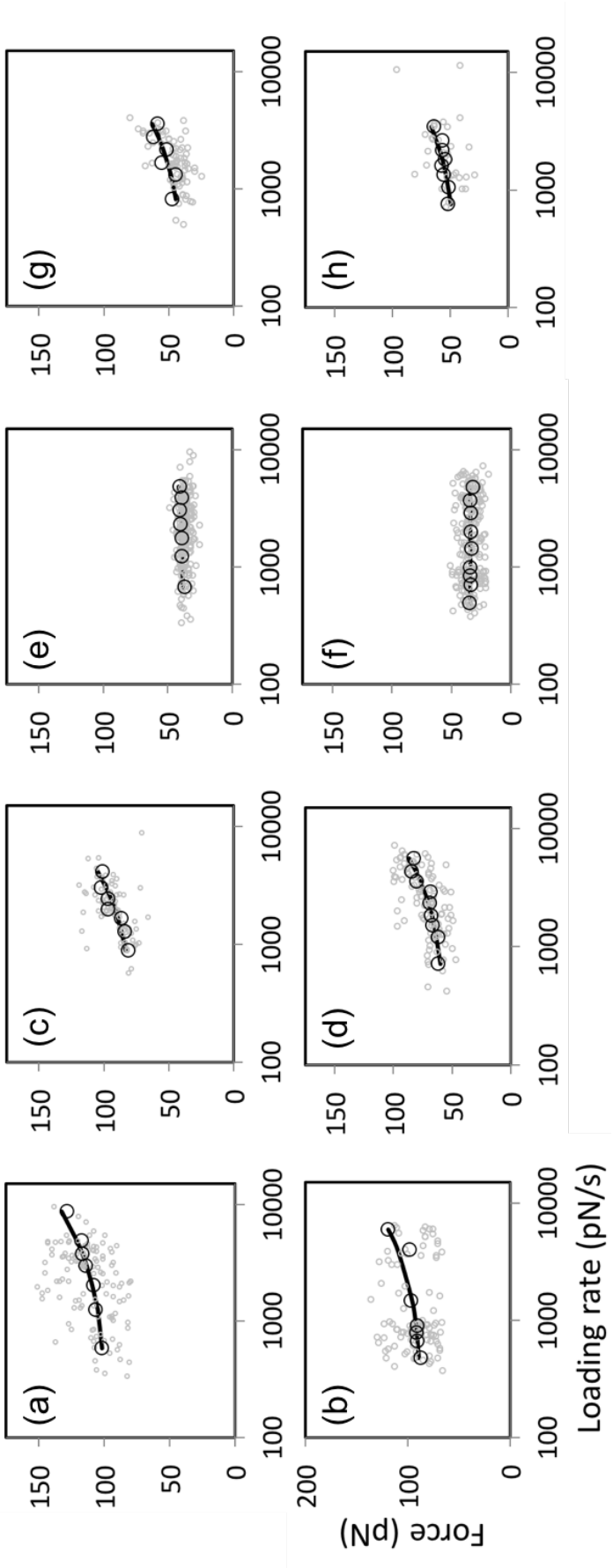
(a)
(b)
(c)
(d)
(e)
(f)
(g)
(h)
Force (pN)
Loading rate (pN/s)
0
50
100
150
200
100
1000
10000

Figure S5.

Figure S5. Dynamic Force Spectra (DFS) plots of Force (pN) vs. Loading rate (pN/s) for sliding events for (a) α-CD and (b) β-CD over station 1; (c) α-CD and (d) β-CD over station 2; (e) α-CD and (f) β-CD over station 3; (g) α-CD over station 4 and (h) α-CD over station 5. Note the logarithmic scale of the *x*-axis. Open circles represent most probable rupture forces in intervals of loading rate, solid lines represent fits of equation S1 to the data.

1.2 Dynamic Force Spectroscopy Analysis

The data selected by the above criteria was ordered by loading rate into bins of equal width and histograms of the rupture forces in each loading rate bin were fit by Gaussian distributions. The most probable rupture forces predicted by these Gaussian fits were then used to construct a dynamic force spectrum, as presented in **Figure S5**. This spectrum was then fit by the Friddle-Noy method [S5, S6] in order to extract values for the free parameters k_{off} and x_t (the intrinsic unbinding rate of the bond and the distance to the transition state, respectively) using equations S1 and S2, as well as a third parameter, the equilibrium force f_{eq} (the minimum force required to move the binding pair apart by the distance x_t, beyond which they can no longer instantaneously rebind). From f_{eq} may be obtained ΔG_{bu}, the free energy of unbinding, for the bond using equation S3 [S5, S6]. All fits to the data were carried out using OriginPro™ (OriginLab, ver. 8.0724).

$$\langle f \rangle \cong f_{eq} + f_{\beta}.ln\left(1 + e^{-\gamma}.\frac{r}{f_{\beta}.k_{u(f)}}\right) \tag{S1}$$

Here $\langle f \rangle$ is the mean rupture force, $f_{\beta} = k_BT/x_t$ is the thermal force scale, k_BT is the Boltzmann constant multiplied by the temperature, $\gamma = 0.577\ldots$ is Euler's constant and r is the loading rate. Values of the parameters x_t, $k_{u(f)}$ (the unbinding constant at *f*) and f_{eq} were obtained from the fit of equation S1 to the data, while k_{off} was obtained from the value of $k_{u(f)}$ and equation S2:

$$k_{off} = {k_{u(f)}}\Big/{exp\left[\frac{\left(f_{eq} - \frac{1}{2}k_{eff}.x_t\right)}{f_{\beta}}\right]} \tag{S2}$$

where k_{eff} is the effective spring constant of the system comprising the cantilever stiffness k_c and the linker stiffness k_l; $k_{eff} = k_c.k_l/(k_c+k_l)$. A value of 0.067 Nm^{-1} was used for the linker

stiffness [S3]. From the values of f_{eq} and k_{eff} the value of ΔG_{bu} can be calculated using equation S3, using the terms already defined above:

$$\Delta G_{bu} = \frac{(f_{eq})^2}{2k_{eff}} \tag{S3}$$

Values of x_t, k_{off}, f_{eq} and ΔG_{bu} were found from the fits of equations S1-3 to the data and presented in **Table S1**. For station 3, no dependence of $\langle f \rangle$ on r is observed so x_β and k_{off} cannot be calculated. **Figure S5** shows the dynamic force spectra and fits to equation S1. In the cases where we are analysing SCFS data, the sliding force term ΔG_{sl} is identical to the term ΔG_{bu} used above.

Table S1. Fitted parameter values for the F-N-Y fit to the dynamic force spectra for stations 1, 2, 4 and 5.

Station	**Bead**	**k_{off} (/s)**	**x_t (nm)**	**f_{eq} ± sd (pN)**	**k_c (pN/nm)**	**ΔG_{bu} ± sd (kJ/mol)**
1	α-CD	8.4	0.10	98 ± 8	25	159 ± 17
	β-CD	14.4	0.08	86 ± 23	22	134 ± 26
2	α-CD	14.6	0.08	76 ± 6	25	95 ± 13
	β-CD	26.1	0.08	63 ± 12	22	72 ± 14
3	α-CD	-	-	29 ± 4 - 37 ± 3	14-25	22 ± 4 - 23 ± 4
	β-CD	-	-	34 ± 5	22	21 ± 6
4 [e]	α-CD	28.9	0.09	45 ± 5	14	54 ± 12
5 [e]	α-CD	23.1	0.10	46 ± 7	16	52 ± 15

Equation S4 is the result of rearranging equation S1 [S5], so that we can conveniently test the validity of S1 graphically by plotting the terms in the equation against each other; a linear fit with a gradient close to 1 implies the validity of equation S1. **Figure S6** shows this plot for stations 1, 2, 4 and 5.

$$e^{-\gamma}.R(0) \cong e^{\langle f \rangle / f_\beta} - e^{f_{eq} / f_\beta}, \tag{S4}$$

$$R(0) = \frac{r}{f_\beta . k_{off}} \tag{S4a}$$

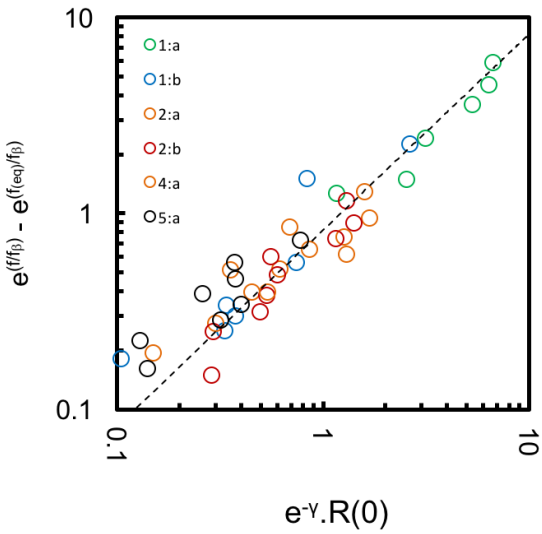

Figure S6. Plot of the same data shown in Figure S4 (a-d and g-h), plotted in the natural coordinates of equation S1, showing the collapse of the data onto a straight line. The dashed line is a linear fit to the data, with slope = 0.82 (R^2 = 0.97).

1.3. Calculating ΔG_{bu} values for the data published by Auletta et al [S7]

Auletta et al. (reference 31 in the main text) provide data on the observed rupture forces (and their lack of dependence on loading rate, implying that these are equilibrium forces) and a range of values for the spring constants of the probes used for their force measurements, so we are able to estimate values of ΔG_{bu} for the rupture of complexes between the guest molecules they studied and β-CD using equation S3. **Table S2** reports these values, together with the same calculations based on the estimated forces simulated by Qamar et al [S8] for the sliding of β-CD over purine and pyrimidine DNA nucleotides.

Table S2. Calculated values of ΔG_{bu} using the reported values of f_{eq} and k_c (0.05-0.12 N/m) in Auletta et al [S7], and in Qamar et al (k_c = 0.3 N/m) [S8].

Guest	**f_{eq} ± sd (pN)**	**ΔG_{bu} ± sd (kJ/mol)**
anilyl	39 ± 15	12.7 ± 9.5
toluidyl	45 ± 15	16.9 ± 10.9
ferrocenyl	55 ± 10	25.3 ± 8.9
tert-butylphenyl	89 ± 15	66.1 ± 30.9
adamantyl	102 ± 15	86.8 ± 24.7
purines	75	31
pyrimidines	78	33

2. UV Measurements of Equilibrium constant K

In order to explore the nature of the relationship between the observed free energy of sliding and the equilibrium constant K for host:guest complexation we collected values of K for the host:guest complexes studied. Literature values are reported for stations 2, 3, 4 and 5 with α- and β-CD (references 22-25 in the main text). To the best of our knowledge the equilibrium constants for the host:guest complex between station 1 and α- and β-CDs have not previously been reported, so we measured K for stations 1 and 2 using the UV spectroscopic method presented below. All values of log K are presented in **Table 1** in the main text.

We employed a spectroscopic method that takes advantage of the red shift in the wavelength of maximum absorption (λ_{max}) and corresponding increase in molar absorption coefficient (ε) that is observed when an aromatic group is included in a CD host in aqueous conditions [S9]. UV spectra are obtained for solutions with a fixed guest concentration [G] and a varied host concentration [CD], and the absorbances at λ_{max} of the uncomplexed guest and at a background wavelength away from the peak in absorbance are recorded. Initially, in order to most closely replicate the situation addressed by the AFM experiments, we sought to measure the complexation of CD with PEG-tethered stations 1 and 2. In each case we observed no, or very little, shift in the UV spectra, suggesting that no complexation between the CDs and stations 1 or 2 occurred. This may be because the CDs preferentially complexed with the PEG, and since PEG lacks chromophores detectable by UV-vis spectroscopy no signal was observed. When, instead, stations 1 and 2 were introduced to CD alone, we observed shifts in the spectra as shown in **Figure S7**. Where such a system exhibits a 1:1 stoichiometry with the host CD, the equilibrium constant K can be evaluated using equation S5:

$$K = \frac{[CD \cdot G]}{[CD].[G]} \tag{S5}$$

Using the well-known Benesi-Hildebrand method [S10], we see that equation S6 describes a linear relationship between $1/\Delta A_i$ and 1/[CD], with a slope of 1/(ΔA.K) and an intercept of 1/ΔA, so that the ratio of intercept to slope yields K. Here, ΔA_i is the difference in absorption at λ_{max} between the guest alone and the guest:host complex and ΔA is Δε.b.[G], where $\Delta\varepsilon = \varepsilon_{\infty} - \varepsilon_0$ (difference in molar absorption coefficients for the complex and the guest alone) and b = path length of the UV cell.

$$\frac{1}{\Delta A_i} = \frac{1}{\Delta A} + \frac{1}{\Delta AK} \cdot \frac{1}{[CD]} \tag{S6}$$

The Benesi-Hildebrand method has been shown to produce inaccurate results under some conditions but when K is in the region 50-1000 M^{-1} and Δε is greater than 50 m^2/mol then reliable results are produced [S10]. In the work presented here K varied from 25 to 646 M^{-1} and Δε varied between 13 and 150 m^2/mol, so the method used may have introduced some errors. Where literature data (derived from calorimetric titration) is available for the aminoaniline (station 2) complexation with α- and β-CD [S11], our result is in broad agreement (log K = 1.47 and 1.41 respectively for our experiments and the literature value for the complexation of aminoaniline and α-CD, and for aminoaniline:β-CD log K = 1.74 and 2.05 respectively for our experiments and the literature value).

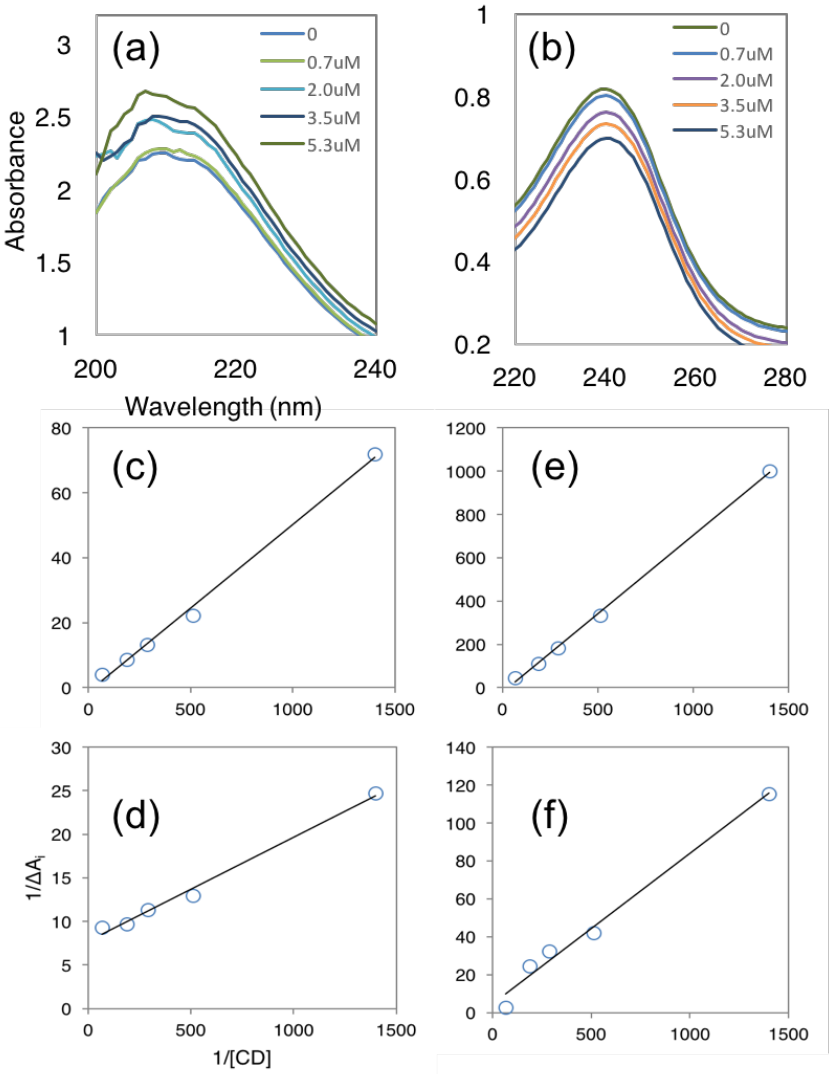

Figure S7. UV spectra for (a) station 1 (aminoaniline) and (b) station 2 (pyromellitic acid) complexing with CD at concentrations ranging from 0 to 5.3 μM. Benesi-Hildebrand plots for the complexation of (c,d) station 1 with α- and β-CD; (e,f) station 2 with α- and β-CD.

3. Calculating the dimensionless space-filling parameter Φ

The dimensionless space-filling parameter Φ is the ratio of the cross-sectional area of the monomer, A, and the cavity area of the CD used (20.18 $Å^2$ for α-CD and 32.95 $Å^2$ for β-CD [S12]). Privalko [S13] proposed a set of equations to allow the calculation of A from m_0, the monomer molecular mass per main chain bond, depending on its expected crystalline conformation (extended chain, EC, equation S7a; helical chain, HC_1, equation S7b; helical chain with bulky sidegroups, HC_2, equation S7c; constants of proportionality k and k' have numerical values of 1 but dimensions of $L^2/M^{0.5}$ (S7a) and L^2/M (S7b and c)):

$$A = k.4.65\sqrt{m_0} \quad \text{(S7a)}$$

$$A = k^{\prime}\ .1.41m_0 \quad \text{(S7b)}$$

$$A = k^{\prime}\ .2.05m_0 \quad \text{(S7c)}$$

Following the assignments made in the literature [S13], all the stations studied here would be expected to adopt the HC_1 conformation, so equation S7b is appropriate. Table S3 presents the calculated values of A and Φ for the stations and CDs used in this work.

Table S3. Calculated values of A and Φ for stations 1-5 and α- and β-CD.

Station	**Monomer MW**	**No. main chain bonds**	**A ($Å^2$)**	**Φ (α-CD)**	**Φ (β-CD)**
1	254.15	6	59.73	2.96	1.81
2	108.144	5	30.50	1.51	0.93
3	44.05	3	20.70	1.03	0.63
4	194.13	5	54.74	2.71	n.d.
5	194.13	5	54.74	2.71	n.d.

Dependences of ΔG_{sl} on Φ and P

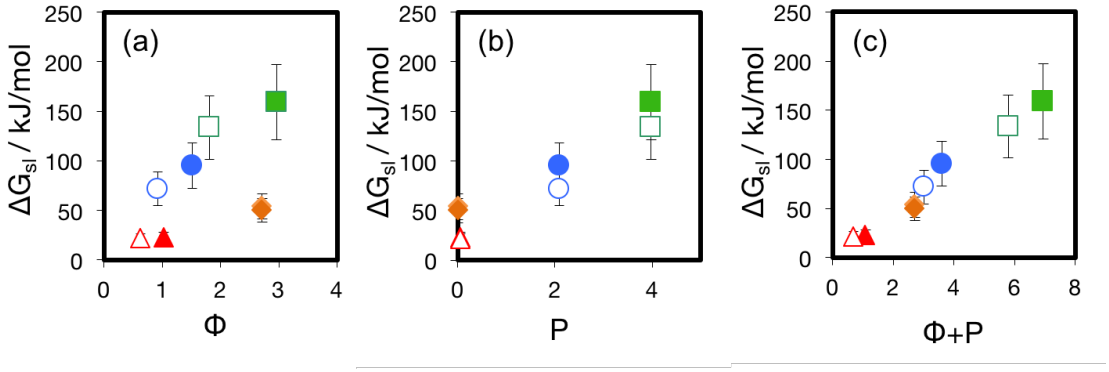

Figure S8. Plots of the relationships between ΔG_{sl} and (a) Φ; (b) P; and (c) Φ+P. Colours of datapoints follow the pattern used in figure 3 in the main text.

Table S4. Calculated values of P, Φ, ΔG_{sh} and f_{eq} for selected monomers and their interactions with α- and β-CD.

	P ($\times 10^{-4}$)	Φ	ΔG_{sh} (kJ/mol)	f_{eq} (pN)
nucleotides and modifications (β-CD)*				
adenosine monophosphate	10.2	3.6	71.6	65.8
thymidine monophosphate	575.4	3.3	68.2	64.2
cytidine monophosphate	7.2	3.4	66.8	63.5
methylcytidine monophosphate	17.0	3.5	68.9	64.6
guanosine monophosphate	7.6	3.8	75.6	67.6
Glycans (α-CD)				
xylose	50.1	1.8	34.8	45.9
glucuronoxylose disaccharide*	1.8	5.5	109.6	81.6
polyhydroxyalkanoates (α-CD)				
polylactic acid	3388	2.1	50.3	55.1
polyglycolic acid	912	1.8	37.4	47.6
Polyhydroxybutyric acid	4074	1.8	46.5	53.0
Polyhydroxyvaleric acid	13804	2.1	76.3	67.9
Polycaprolactone	23442	1.3	86.3	72.2
Polyhydroxypropylmethacrylamide	13490	5.1	135.1	90.4
amino acids and modifications (α-CD)				
arginine	6.9	4.1	80.4	69.7
histidine	2.4	3.6	71.6	65.8
lysine	6.2	3.4	67.5	63.9
aspartic acid	3.2	3.1	61.4	60.9
glutamic acid	5.8	3.4	67.9	64.1
serine	1.3	2.4	48.5	54.2
phosphoserine	6.6	4.3	85.5	71.9
O-glycosylserine*	2.0	8.8	174.6	102.8
threonine	3.4	2.8	55.0	57.7
phosphothreonine	20.0	4.6	92.0	92.0
O-glycosylthreonine*	2.0	9.3	184.0	105.5
asparagine	0.5	3.1	61.0	60.7
N-acetylglucosylaminoasparagine*	2.0	10.3	203.5	110.9
glutamine	1.0	3.4	67.4	63.8
cysteine	16.2	2.8	55.9	58.1
glycine	3.8	1.7	34.7	45.8
proline	26.9	2.7	53.2	56.7

alanine	14.5	2.1	41.2	49.9
valine	109.6	2.7	54.3	57.3
isoleucine	309.0	3.1	61.3	60.9
leucine	257.0	3.1	61.2	60.8
methionine	64.6	3.5	69.0	64.6
phenylalanine	645.7	5.6	112.5	82.5
tyrosine	316.2	6.1	122.4	86.0
phosphotyrosine	309.0	8.8	176.1	103.2
tryptophan	812.8	6.9	139.1	91.7

* Φ calculated using equation S7c

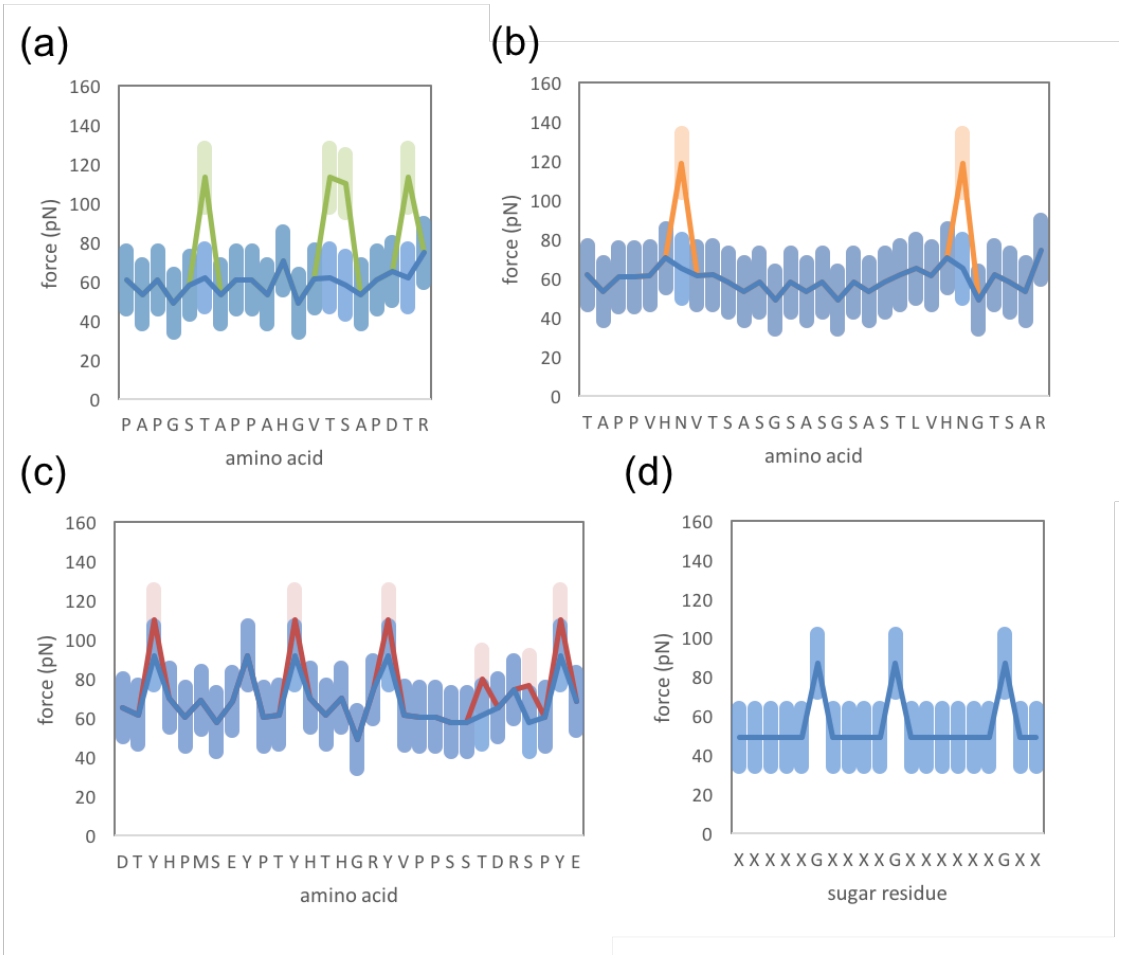

Figure S9. Plots of predicted force vs. sequence for (a) O-glycosylation of the 20 a.a. tandem repeat in the human protein MUC-1 (glycosylated sequence in green, unmodified sequence blue); (b) N-glycosylation of the region 951-980 in MUC-1 (glycosylated sequence in orange, unmodified sequence blue); (c) phosphorylation of the region 1201-1230 in MUC-1(phosphorylated sequence in red, unmodified sequence blue); (d) glucuronic acid decoration of the xylan backbone in a hypothetical glucuronoxylan sequence. In all cases solid lines show mean predicted force for a cantilever with k_c = 25 pN/nm, error bars represent ±15 pN.

4. Gel Permeation Chromatography (GPC)

Gel permeation chromatography (GPC) with refractive index detection (PL aquagel-OH 30 (Agilent Technologies, Santa Clara, CA, USA) column with a low flow rate of 0.3 ml/min and a run time of 40 min) was used to determine the increase in molecular weight and so establish the success of the conjugation between oligomers of stations 4 and 5 (guluronic and mannuronic acids) and PEG. Calibration of the GPC retention time with respect to molecular weight was carried out using two polymer series: PEGs coupled to maltose and a series of guluronate oligomers. Different relationships between molecular weight and retention time were found for the two series (**figure S10**). Calculation of the molecular weight of the guluronate -PEG conjugate used in the AFM experiments was carried out using the linear fits to the two polymer series in proportion to the contribution of each polymer to the overall molecular weight of the conjugate. The PEG alone was retained at t=25.82 mins, corresponding to a mass of 2500 Da and the guluronates were retained at t = 24.68 mins, corresponding to a mass of 1750 Da.

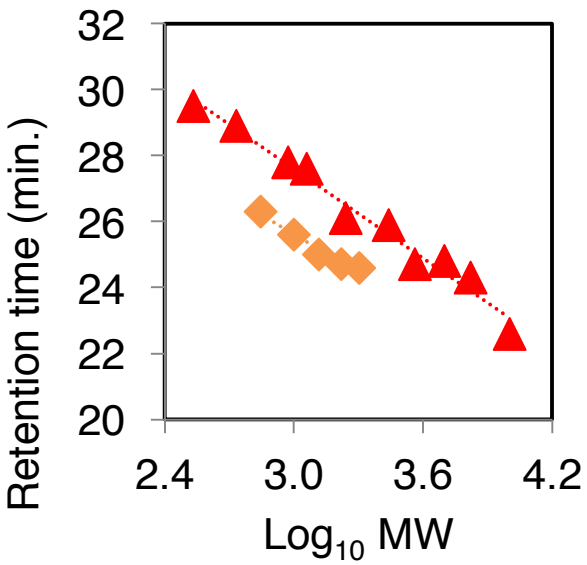

Figure S10. Plot of retention time vs. log MW for a series of PEG-maltose conjugates (red triangles) and a series of guluronate oligomers (orange diamonds).

Guluronate-PEG conjugates were then run on the column, giving rise to the retention profiles presented in **figure S11**. Retention times for the PEG-alginate conjugate are shorter than for PEG alone, and reach a maximum after 48 hours. The retention time reached after 72 hours is

24.2 minutes, which for a conjugate consisting of 60% w/w PEG and 40% w/w alginate oligomer corresponds to a mass of approximately 3600 Da. This value is in reasonable agreement (85%) with the predicted mass of the conjugate.

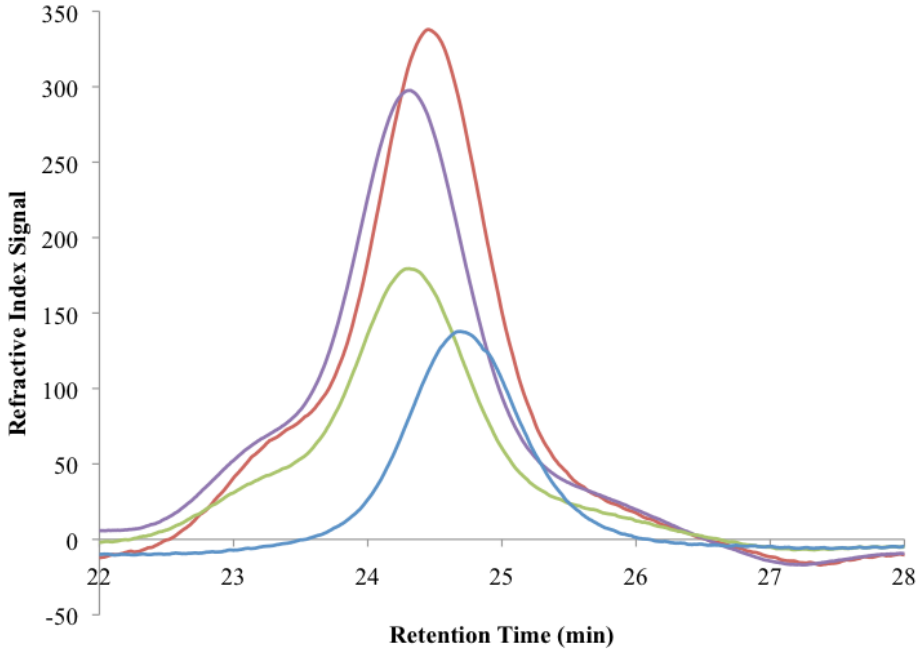

Figure S11. Retention times of a mannuronic acid decamer and its conjugates with a 2500 MW diamino-functionalised PEG. Blue trace is mannuronate alone, red, purple and green traces are the conjugate after 24, 48 and 72 hours reaction time.

Readers may request access to the data used to prepare this manuscript from the corresponding author at the following email address: a.round@uea.ac.uk

References

[S1] A. Janshoff, M. Neitzert, Y. Obersörfer, and H. Fuchs, *Angew. Chem. Int. Ed.,* 2000, **39**, 3212.

[S2] A. Dunlop, J. Wattoom, E. A. Hasan, T. Cosgrove and A. N. Round, *Nanotechnology*, 2008, **19**, 345706

[S3] F. Oesterhelt, M. Rief, and H. E. Gaub, *New Journal of Physics* 1999, **1**, 6.

[S4] S. Guo, N. Li, N. Lad, S. Desai, and B. B. Akhremitchev, *Journal of Physical Chemistry C*, 2010, **114**, 8755.

[S5] R. W. Friddle, A. Noy, and J. J. De Yoreo, *PNAS*, 2012, **109**, 13573.

[S6] A. Noy, and R. W. Friddle, *Methods*, 2013, **60**, 142.

[S7] T. Auletta, M. R. de Jong, A. Mulder, F. C. J. M. van Veggel, J. Huskens, D. N. Reinhoudt, S. Zou, S. Zapotoczny, H. Schonherr, G. J. Vancso and L. Kuipers, *J Am Chem Soc*, 2004, **126**, 1577–1584.

[S8] S. Qamar, P. M. Williams and S. M. Lindsay, *Biophys J*, 2008, **94**, 1233–1240.

[S9] M. V. Rekharsky and Y. Inoue, *Chemical Reviews*, 1998 **98(5)**, 1875–1918.

[S10] C. Yang, C., L. Liu, L., T.-W. Mu and Q.-X. Guo, *Analytical Sciences*, 2000 **16(5),** 537–539.

[S11] H. J. Buschmann, K. Jansen and E. Schollmeyer, *Journal of inclusion …*, 2000.

[S12] G. Wenz, B. Han and A. Muller, *Chem Rev*, 2006, **106**, 782–817

[S13] V. Privalko, *Macromolecules*, 1980, **13**, 370–372